Monthly Notices of the ROYAL ASTRONOMICAL SOCIETY

MNRAS **496,** 851–863 (2020)
Advance Access publication 2020 June 3

doi:10.1093/mnras/staa1528

K2-HERMES II. Planet-candidate properties from K2 Campaigns 1-13

Robert A. Wittenmyer,[1★] Jake T. Clark,[1] Sanjib Sharma,[2] Dennis Stello,[3] Jonathan Horner,[1] Stephen R. Kane,[4] Catherine P. Stevens,[5] Duncan J. Wright,[1] Lorenzo Spina,[6] Klemen Čotar,[7] Martin Asplund,[8] Joss Bland-Hawthorn,[2] Sven Buder,[8,9,10] Andrew R. Casey,[6] Gayandhi M. De Silva,[2] Valentina D'Orazi,[11] Ken Freeman,[8] Janez Kos,[2] Geraint Lewis,[2] Jane Lin,[2] Karin Lind,[10,12] Sarah L. Martell,[3,9] Jeffrey D. Simpson,[3] Daniel B. Zucker[13,14] and Tomaz Zwitter[7]

[1]*University of Southern Queensland, Centre for Astrophysics, USQ Toowoomba, Toowoomba, QLD 4350, Australia*
[2]*Sydney Institute for Astronomy, School of Physics, University of Sydney, Sydney, NSW 2006, Australia*
[3]*School of Physics, University of New South Wales, Sydney, NSW 2052, Australia*
[4]*Department of Earth and Planetary Sciences, University of California, Riverside, CA 92521, USA*
[5]*Department of Physics, Westminster College, New Wilmington, PA 16172, USA*
[6]*Monash Centre for Astrophysics, School of Physics and Astronomy, Monash University, Monash, VIC 3800, Australia*
[7]*Faculty of Mathematics and Physics, University of Ljubljana, Jadranska 19, 1000 Ljubljana, Slovenia*
[8]*Research School of Astronomy and Astrophysics, Australian National University, Canberra, ACT 2611, Australia*
[9]*ARC Centre of Excellence for All Sky Astrophysics in 3 Dimensions (ASTRO 3D), Canberra, ACT 2611, Australia*
[10]*Max Planck Institute for Astronomy (MPIA), Koenigstuhl 17, D-69117 Heidelberg, Germany*
[11]*INAF Osservatorio Astronomico di Padova, vicolo dell'Osservatorio 5, I-35122 Padova, Italy*
[12]*Department of Physics and Astronomy, Uppsala University, Box 516, SE-751 20 Uppsala, Sweden*
[13]*Department of Physics and Astronomy, Macquarie University, Sydney, NSW 2109, Australia*
[14]*Research Centre in Astronomy, Astrophysics and Astrophotonics, Macquarie University, Sydney, NSW 2109, Australia*

Accepted 2020 May 21. Received 2020 May 20; in original form 2020 March 10

ABSTRACT

Accurate and precise radius estimates of transiting exoplanets are critical for understanding their compositions and formation mechanisms. To know the planet, we must know the host star in as much detail as possible. We present complete results for planet-candidate hosts from the K2-HERMES survey, which uses the HERMES multi-object spectrograph on the Anglo-Australian Telescope to obtain $R \sim 28\,000$ spectra for more than 30 000 K2 stars. We present complete host-star parameters and planet-candidate radii for 224 K2 candidate planets from C1–C13. Our results cast severe doubt on 30 K2 candidates, as we derive unphysically large radii, larger than $2R_{\rm Jup}$. This work highlights the importance of obtaining accurate, precise, and self-consistent stellar parameters for ongoing large planet search programs – something that will only become more important in the coming years, as *TESS* begins to deliver its own harvest of exoplanets.

Key words: techniques: spectroscopic – planets and satellites: fundamental parameters – stars: fundamental parameters.

1 INTRODUCTION

With the discovery of the first planets orbiting other stars (Campbell, Walker & Yang 1988; Latham et al. 1989; Wolszczan & Frail 1992; Mayor & Queloz 1995), humanity entered the 'Exoplanet Era'. For the first time, we had confirmation that the Solar system was not unique, and began to realize that planets are ubiquitous in the cosmos (e.g. Fressin et al. 2013; Winn & Fabrycky 2015; Hardegree-Ullman et al. 2019). At the same time, we learned that planetary systems are far more diverse than we had previously imagined. We discovered planets denser than lead and more insubstantial than candy floss (Burgasser et al. 2010; Masuda 2014; Johns et al. 2018; Raetz et al. 2019), found a myriad of systems containing giant planets orbiting perilously close to their host stars (e.g. Mayor & Queloz 1995; Masset & Papaloizou 2003; Bouchy et al. 2005; Hellier et al.

★ E-mail: rob.w@usq.edu.au

2011; Albrecht et al. 2012; Wright et al. 2012), and discovered others with planets moving on highly elongated, eccentric orbits, similar to those of comets in the Solar system (e.g. Wittenmyer et al. 2007; Tamuz et al. 2008; Harakawa et al. 2015; Wittenmyer et al. 2017). We even uncovered two types of planets that have no direct analogue in the Solar system – the super-Earths and sub-Neptunes (e.g. Charbonneau et al. 2009; Vogt et al. 2010; Winn et al. 2011; Howard et al. 2012; Sinukoff et al. 2016).

The rate at which we found new exoplanets was boosted dramatically by the launch of the *Kepler* spacecraft in 2009. In the years that followed, *Kepler* performed the first great census of the Exoplanet Era. In doing so, it revolutionized exoplanetary science, discovering some 2347 validated planets,[1] and finding hundreds of multiply-transiting systems (e.g. Borucki et al. 2010; Batalha et al. 2013; Mullally et al. 2015). After the failure of its second reaction wheel in 2013, the spacecraft was repurposed to carry out the 'K2' mission (Howell et al. 2014). *Kepler's* golden years were spent in ∼80-d observations of fields along the ecliptic plane, with targets selected by the broader astronomical community for a wide range of astrophysical studies beyond planet search. A total of 20 pointings ('campaigns') were performed until the spacecraft station-keeping fuel was exhausted in 2018 October. Altogether, the K2 mission observed more than 150 000 stars across 20 campaigns, resulting in 397 confirmed and 891 candidate planets to date.[2]

With the exception of the small number of directly imaged exoplanets (e.g. Kalas et al. 2008; Marois et al. 2008, 2010; Lagrange et al. 2009), our knowledge of the new worlds we discover has been gleaned indirectly. We observe a star doing something unexpected, and infer the presence of a planet. Our knowledge of the planets we find in this manner is directly coupled to our understanding of their host stars. For example, consider the case of a planet discovered using the transit technique. By measuring the degree to which the light of the planet's host star is attenuated during the transit, it is possible to infer the planet's size. The larger the planet, the more light it will block, and the greater the dimming of its host star. As a result, it is relatively straightforward to determine the size of the planet *relative to its host star*. When converting those measurements to a true diameter for the newly discovered world, however, one must base that diameter on the calculated/assumed size of the host star. Any uncertainty in the size of the host carries through to the determination of the size of the planet.

For that reason, it is critically important for us to be able to accurately characterize the stars that host planets. The more information we have about those stars, and the more precise those data, the more accurately we can determine the nature of their orbiting planets.

Over the past few years, the Galactic Archaeology with HERMES survey (GALAH) has been gathering highly detailed spectra of a vast number of stars in the local Solar neighbourhood (e.g. De Silva et al. 2015; Martell et al. 2017; Buder et al. 2018). The survey uses the High Efficiency and Resolution Multi-Element Spectrograph (HERMES) on the Anglo-Australian Telescope (Freeman 2012; Simpson et al. 2016) to simultaneously obtain approximately 400 spectra in a given exposure. Analysis of those high-resolution spectra allows the determination of a variety of the properties of those stars, along with the calculation of accurate abundances for up to thirty different elements in their outer atmospheres. GALAH aims to survey a million stars, facilitating an in-depth study of our Galaxy's star formation history – and has already yielded impressive results (e.g. Duong et al. 2018; Gao et al. 2018; Quillen et al. 2018; Zwitter et al. 2018; Kos et al. 2018a,b; Čotar et al. 2019a,b; Žerjal et al. 2019). Whilst the data obtained by the GALAH survey is clearly of great interest to stellar and Galactic astronomers, it can also provide information of critical importance to the exoplanet community. For that reason, in this work we describe the results of the K2-HERMES survey, whose design follows that of the main GALAH program, but is designed specifically to maximize the scientific value of the plethora of exoplanets and oscillating stars discovered during *Kepler's* K2 mission (Wittenmyer et al. 2018; Sharma et al. 2019).

K2-HERMES is a survey born out of the urgent need for accurate, precise, and self-consistent physical parameters for stars including those hosting candidate planets. Using the same instrumental setup and data processing pipelines as GALAH, the K2-HERMES survey aims to collect a spectrum for as many K2 target stars as possible in a given colour–magnitude limited sample. For each target so observed, we compute spectroscopic stellar parameters ($T_{\rm eff}$, log g, [Fe/H]), as well as the derived physical parameters such as mass, radius, luminosity, and age. The HERMES instrument was specifically designed to measure the chemical abundances of up to thirty elements for the GALAH survey, and so those abundances are also delivered by the standard GALAH data processing pipeline. A forthcoming paper, Clark et al. (in preparation), will present a detailed analysis of the chemical abundance results in the context of the *Transiting Exoplanet Survey Satellite* mission, *TESS*.

In this paper, we present the complete results of planet-candidate properties from the K2-HERMES survey for K2 campaigns 1-13. In Section 2, we briefly describe the observing strategy and data analysis procedures, and we detail how the stellar physical parameters have been derived. Section 3 gives the physical properties of the K2 planet candidates and their host stars. Finally, in Section 4, we place our results in context and present our conclusions.

2 OBSERVATIONS AND DATA ANALYSIS

Target selection for the K2-HERMES program is described fully in our previous work (Wittenmyer et al. 2018; Sharma et al. 2019). Fig. 1 shows the HERMES field of view overlaid on the *Kepler* field. For this study, we selected all K2 planet candidate host stars which had been observed in the K2-HERMES program.

2.1 Determination of stellar parameters

We find 199 stars hosting 224 K2 planet candidates for which K2-HERMES spectra are available. The reduction and analysis procedures are identical to those of the GALAH and TESS-HERMES surveys, as described fully in Kos et al. (2017), Buder et al. (2018), and Sharma et al. (2018).

With a self-consistent set of spectroscopic parameters in hand ($T_{\rm eff}$, log g, [Fe/H]), we derived the stellar physical parameters using the `isochrones` Python package (Morton 2015). `isochrones` is a Bayesian isochronic modeller that determines the mass, radius, and age of stars given various photometric and spectroscopic inputs using MESA Isochrones & Stellar Tracks (MIST) (Dotter 2016) grids. For our analysis, we used the effective temperature ($T_{\rm eff}$), surface gravity (log g), 2MASS (H, J, K_s) (Skrutskie et al. 2006), and *Gaia* (G, G_{RP}, G_{BP}) photometric magnitudes along with parallax

[1] as of 2020 February 26, from the NASA Exoplanet Archive, https://exoplanetarchive.ipac.caltech.edu/. A further 2420 candidate planets were found during the *Kepler* main mission, and still await confirmation.
[2] Planet data obtained from the NASA Exoplanet Archive, accessed 2020 February 26, at https://exoplanetarchive.ipac.caltech.edu/

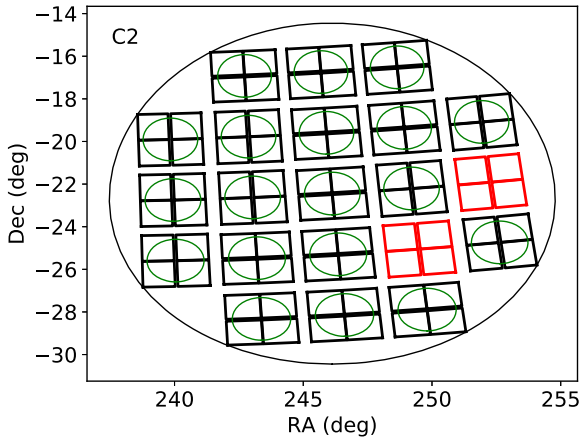

Figure 1. The *Kepler* field of view and the layout of its CCD modules, overlaid with the HERMES field of view (green circles). The red modules are inoperative.

values obtained by *Gaia* DR2 (Gaia Collaboration 2018) where available.

Accurate isochrone models rely upon a star's global metallicity, commonly referred as [M/H]. The assumption that the iron abundance [Fe/H] can be a proxy (or even equal) to [M/H] breaks down for metal-poor stars. In these metal-poor stars, the radiative opacity can be heavily affected by alpha-elements, in our case Mg, Si, Ca, and Ti. Including alpha-elements into our global metallicity thus better predicts the physical parameters derived with `isochrones`. We calculate our [α/Fe] values through equation (1), which is the exact procedure taken by GALAH DR2:

$$[\alpha/Fe] = \frac{\sum \frac{[X/Fe]}{(e\_[X/Fe])^2}}{\sum (e\_[X/Fe])^{-2}}, \quad (1)$$

where X = Mg, Si, Ca, Ti, and e_[X/Fe] is the abundance's associated error. [α/Fe] is calculated even if one or more of these elements are missing. From [Fe/H] and [α/Fe], we can then calculate [M/H] through a relationship between these quantities laid out in Salaris, Chieffi & Straniero (1993):

$$[M/H] = [Fe/H] + \log_{10}\left(0.638 * f_\alpha + 0.362\right), \quad (2)$$

where f_α is the α-element enhancement factor given by $f_\alpha = 10^{[\frac{\alpha}{Fe}]}$. Our calculated [M/H] value is then used for our isochrone star model on top of the discussed parameters above. After the model reaches convergence, median output values of the stellar mass, radius, density, age, bolometric luminosity and equivalent evolution phase and their corresponding 1-σ errors are calculated from the posterior distributions. We calculate the stellar luminosity by:

$$\left(\frac{L}{L_\odot}\right) = \left(\frac{R}{R_\odot}\right)^2 \left(\frac{T}{T_\odot}\right)^4. \quad (3)$$

A Hertzsprung–Russell diagram of our results is shown in Fig. 2, based on our $T_{\rm eff}$, log g, and `isochrones`-derived stellar luminosity. This sanity check confirms that none of our 199 K2 stars fall in unphysical regions of parameter space. Three stars (EPIC 201516974, 211351816, 211390903) show asteroseismic detections of the large frequency separation, $\Delta\nu$, and the frequency at maximum power, $\nu_{\rm max}$. For these detections we used EVEREST K2 light curves (Luger et al. 2016) that we analysed following the approach by Stello et al. (2017), which uses the method by Huber et al. (2009) with the improvements described in Huber et al. (2011) and in Yu et al. (2018). Then, using the seismic $\Delta\nu$ and $\nu_{\rm max}$ and

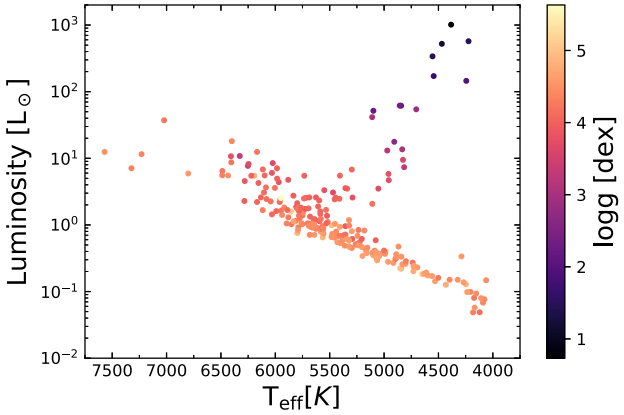

Figure 2. H–R diagram of our K2-HERMES and `isochrones`-derived results for 199 K2 stars.

the methods of Hon, Stello & Yu (2018) and Sharma et al. (2016), we derived physical parameters for these three stars and give them in Table 1 alongside our spectroscopic results from `isochrones`.

The resulting stellar parameters are given in Table 2. Our K2-HERMES results have the following median uncertainties: $T_{\rm eff}$: 74 K, log g: 0.19 dex, [Fe/H]: 0.08 dex, M_*: 0.036 $M_\odot$, R_*: 0.019 $R_\odot$. Figs 3–5 compare our K2-HERMES spectroscopic parameters with those presented by Huber et al. (2016) (based largely on multicolour photometry), and recent results from Hardegree-Ullman et al. (2020) based on LAMOST spectra. Fig. 6 shows the comparison between our derived stellar radii and masses and those of Huber et al. (2016) and Hardegree-Ullman et al. (2020), as well as the radii inferred from *Gaia*.

A primary motivation for refining stellar parameters is to determine which planets would be best suited for follow-up activities (Chandler, McDonald & Kane 2016; Kempton et al. 2018; Ostberg & Kane 2019). This is particularly true of studies related to potentially habitable planets and the effect of stellar properties on the extent of the Habitable Zone (HZ) (Kane 2014, 2018). The stellar parameters derived above were used to estimate several key properties of the known planets and their systems, shown in Table 3. We calculated the incident flux received by the planet in units of the solar constant ($F_\oplus$) using the semimajor axis and stellar luminosity. We further calculated the equilibrium temperature for each planet ($T_{\rm eq}$) using both 'hot dayside' and well-mixed models, which assume that the planet re-radiates as a blackbody over 2π and 4π steradians, respectively (Kane & Gelino 2011). Finally, we calculated the HZ boundaries for each of the stars, using the formalism described by Kopparapu et al. (2013, 2014). We calculated the 'runaway greenhouse' and 'maximum greenhouse' boundaries (referred to as the 'conservative' HZ) and the empirically derived 'recent Venus' and 'early Mars' boundaries (referred to as the 'optimistic' HZ). A thorough description of these boundaries and how they are used is provided by Kane et al. (2016). Although all of the planets whose insolation properties are shown in Table 3 are interior to the HZ, some of the planets do lie in the Venus Zone (VZ) (Kane, Kopparapu & Domagal-Goldman 2014). Terrestrial planets that lie within the VZ are also valued targets for follow-up activities as they can provide insight into the boundaries of habitability and the divergence of the Venus/Earth atmospheric evolution (Kane et al. 2019). Further investigations of these systems may yet reveal additional planets within the HZ of the stars, increasing the value of those systems through comparative planetology studies of planets throughout the system.

Table 1. Stellar parameters derived from seismology, and comparison with the spectroscopic results from K2-HERMES.

EPIC	log *g* Seismology	Radius ($R_\odot$)	Mass ($M_\odot$)	log *g* K2-HERMES	Radius ($R_\odot$)	Mass ($M_\odot$)
201516974	2.934 ± 0.010	5.26 ± 0.16	0.87 ± 0.07	2.69 ± 0.16	5.84 ± 0.25	1.30 ± 0.14
211351816	3.245 ± 0.007	4.11 ± 0.07	1.08 ± 0.05	4.16 ± 0.17	4.42 ± 0.24	1.56 ± 0.15
211390903	2.626 ± 0.022	8.8 ± 0.5	1.19 ± 0.20	2.89 ± 0.19	11.10 ± 0.56	1.73 ± 0.28

Table 2. Spectroscopic and derived stellar parameters. The full version of this table is available online.

EPIC	$T_{\rm eff}$ (K)	log *g*	[Fe/H]	Mass ($M_\odot$)	Radius ($R_\odot$)
201110617	4247.7 ± 465.7	4.83 ± 0.23	−0.17 ± 0.10	0.695 ± 0.020	0.663 ± 0.009
201127519	4737.0 ± 58.1	4.23 ± 0.17	0.15 ± 0.07	0.832 ± 0.026	0.777 ± 0.008
201128338	4205.2 ± 81.0	4.37 ± 0.18	−0.47 ± 0.07	0.610 ± 0.012	0.594 ± 0.007
201132684	5407.0 ± 54.8	4.37 ± 0.17	0.10 ± 0.07	0.915 ± 0.029	0.947 ± 0.013
201155177	4694.2 ± 98.1	4.56 ± 0.21	−0.20 ± 0.09	0.760 ± 0.025	0.727 ± 0.014
201160662	6486.5 ± 68.9	4.25 ± 0.19	−0.81 ± 0.08	1.240 ± 0.072	2.020 ± 0.067
201264302	4181.5 ± 207.5	4.33 ± 0.21	−0.48 ± 0.09	0.446 ± 0.025	0.421 ± 0.006
201390927	4288.2 ± 71.9	4.57 ± 0.19	−0.30 ± 0.08	0.884 ± 0.053	1.050 ± 0.091
201393098	5625.9 ± 73.6	3.94 ± 0.19	−0.34 ± 0.08	1.070 ± 0.039	1.700 ± 0.040
201403446	6132.3 ± 59.9	4.05 ± 0.18	−0.47 ± 0.07	1.060 ± 0.040	1.430 ± 0.034

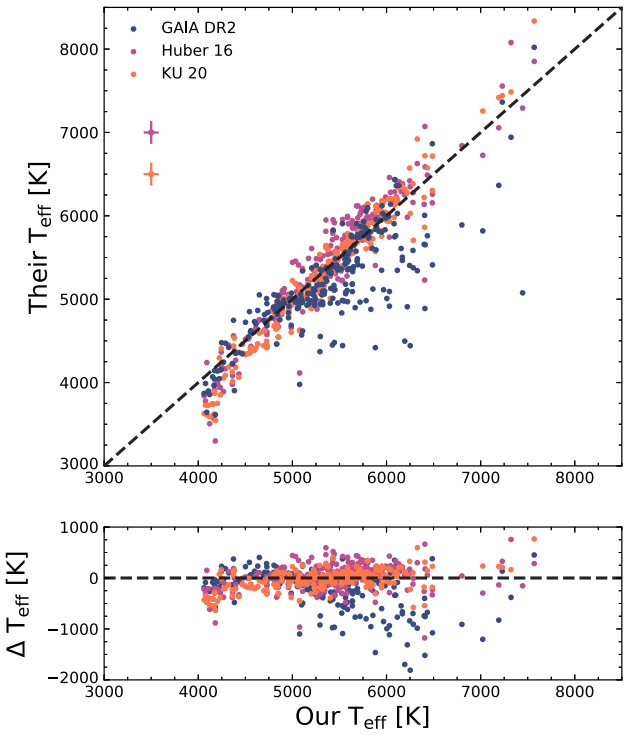

Figure 3. Comparison of our revised $T_{\rm eff}$ with published values. The RMS differences are: *Gaia* – 29 K, H16–16 K, KU20–11 K. Median error bars are also shown.

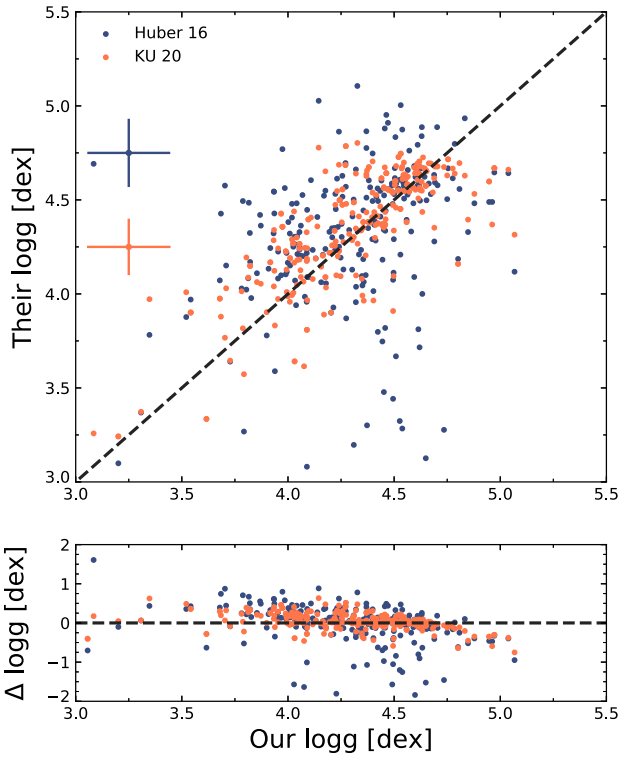

Figure 4. Comparison of our revised log *g* with published values. The RMS differences are: H16–0.03 dex, KU20–0.01 dex. Median error bars are also shown.

3 PLANET CANDIDATE PARAMETERS

Table 4 gives the properties of the 224 planet candidates from C1-C13 for which the K2-HERMES program has obtained spectra of their host stars. The orbital period and relative radius R_p/R_* are obtained from the NASA Exoplanet Archive, with the relevant references cited in Table 4. Where multiple published values exist, the most recent reference was chosen for our analysis. The semimajor axis values have been recalculated based on the orbital period and the revised stellar masses given in Table 2. We derived the planet-candidate radii by multiplying R_p/R_* by the stellar radii obtained by `isochrones` as described above. Uncertainties in the planetary radii result from the propagated uncertainties in R_* and R_p/R_*. As in our previous work (Wittenmyer et al. 2018), for those planet candidates without published uncertainties in R_p/R_*, we adopted the median fractional uncertainty of 0.0025 derived from the catalogue of Crossfield et al. (2016).

Using our self-consistent stellar radii, we find the derived planet-candidate radii to lie in a reasonable range for approximately

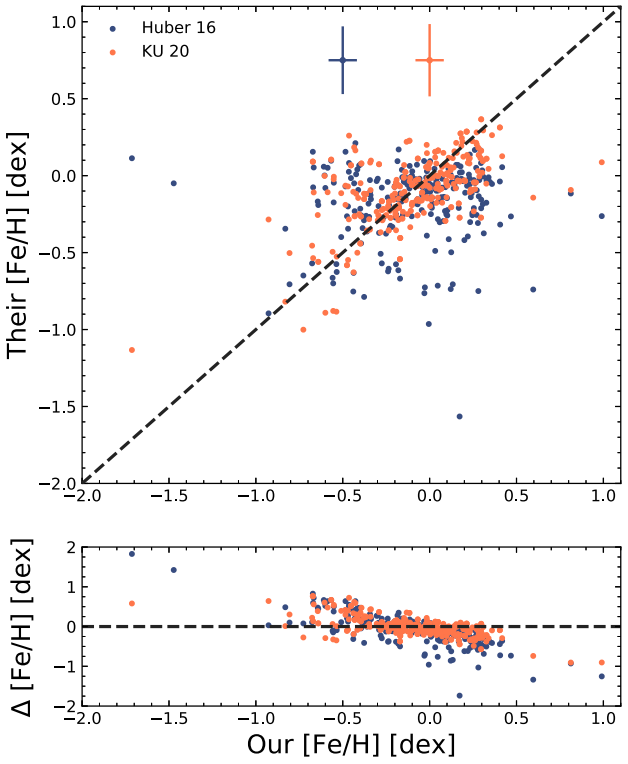

Figure 5. Comparison of our revised [Fe/H] with published values. The RMS differences are: H16–0.02 dex, KU20–0.01 dex. Median error bars are also shown.

90 per cent of the planet candidates examined here. We set an upper limit of $2R_{\rm Jup}$ ($22\,R_\oplus$), a radius larger than which no planet has been confirmed. By this criterion, we find 30 candidates with unphysically large radii, and we strongly suspect them to be false positives. All have a disposition status of 'candidate' (i.e. not 'confirmed') on the NASA Exoplanet Archive, and they are enumerated in Table 5.

We checked the *Gaia* DR2 results for evidence of hidden binarity in these 30 targets. One star (EPIC 203929178) had highly significant excess astrometric noise (hundreds of sigma). A further seven stars had uncertainties in their absolute radial velocities more than 3σ larger than the expected RV precision for stars of their temperature (Katz et al. 2019). We also flag eleven stars as giants with $\log g \lesssim 3.0$ from our spectroscopic determination. Those giant-star hosts are more likely to be false positives, e.g. wherein a grazing eclipse by an M dwarf can produce the *K*2 transit-like signal, or where the transiting object orbits a different star, as postulated by the analysis of *Kepler* giants in Sliski & Kipping (2014). Two stars have a weak secondary set of spectral lines, and are marked as binaries here. None of the 30 stars in Table 5 have K2-HERMES-derived stellar parameters that are unusually imprecise (Table 2), and so we are confident in our disposition of these planetary candidates as false positives due to their unrealistically large inferred radii. Furthermore, two stars in Table 5 have seismic detections confirming their evolved nature. EPIC 211351816, hosting the confirmed planet K2-97b (Grunblatt et al. 2018), also has a seismic detection. We derive its radius to be $4.11 \pm 0.07\,{\rm R}_\odot$ (Table 1), in turn yielding a planetary radius of $11.22 \pm 1.43\,R_\oplus$ which agrees with our K2-HERMES radius determination ($12.07 \pm 1.66\,R_\oplus$),

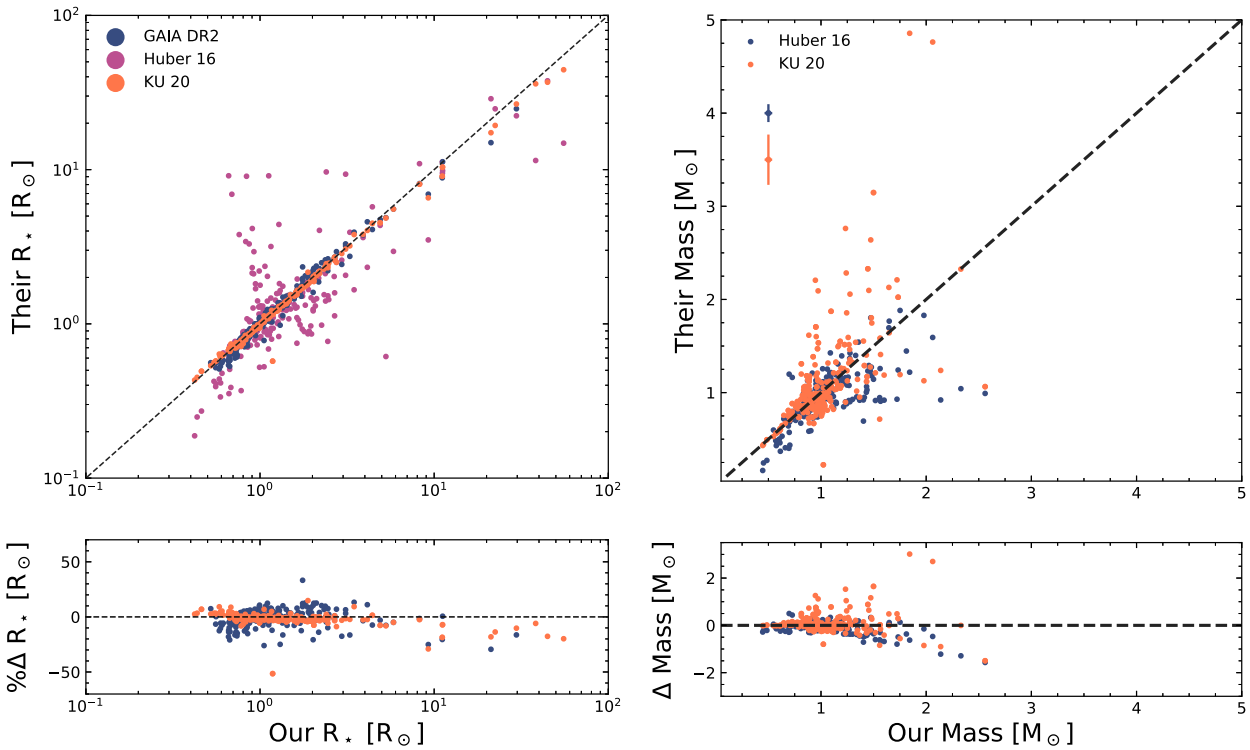

Figure 6. Comparison of our derived stellar physical parameters with published values.

Table 3. Planetary insolation and Habitable Zone boundaries. The full version of this table is available online.

EPIC	Incident Flux $F_\oplus$	T_{eq} (K) hot dayside	T_{eq} (K) well-mixed	HZ (au) inner, opt	HZ (au) inner, conserv	HZ (au) outer, conserv	HZ (au) outer opt
201110617.01	566.1	1616.0	1358.9	0.29	0.37	0.69	0.72
201127519.01	70.9	961.2	808.3	0.41	0.52	0.96	1.01
201128338.01	3.4	451.2	379.4	0.25	0.32	0.60	0.64
201132684.01	178.6	1211.0	1018.3	0.64	0.81	1.44	1.51
201132684.02	87.7	1013.8	852.5	0.64	0.81	1.44	1.51
201155177.01	57.3	911.4	766.4	0.38	0.48	0.88	0.93
201160662.01	8243.2	3156.7	2654.4	1.83	2.31	4.02	4.24
201264302.01	1722.6	2134.3	1794.7	0.18	0.23	0.42	0.45
201390927.01	262.3	1333.2	1121.1	0.47	0.59	1.11	1.17
201393098.01	73.7	970.7	816.3	1.22	1.54	2.73	2.88

Table 4. Planet-candidate properties. References – 1: Mayo et al. (2018), 2: Livingston et al. (2018b), 3: Crossfield et al. (2016), 4: Adams, Jackson & Endl (2016), 5: Vanderburg et al. (2016), 6: Schmitt et al. (2016), 7: Zink et al. (2019), 8: Pope, Parviainen & Aigrain (2016), 9: Dressing et al. (2017), 10: Nardiello et al. (2016), 11: Petigura et al. (2017), 12: Mann et al. (2017), 13: Kruse et al. (2019).

EPIC	K2 ID	Reference	P (d)	a (au)	R_p/R_*	R_p ($R_\oplus$)
201110617	K2-156	1	0.813149 ± 0.000050	0.01510 ± 0.00014	0.017041 ± 0.0014	1.23 ± 0.10
201127519	–	1	6.178369 ± 0.000195	0.06197 ± 0.0006	0.115111 ± 0.0049	9.77 ± 0.43
201128338	K2-152	2	32.6479 ± 0.01483	0.16952 ± 0.00119	0.0344 ± 0.0037	2.23 ± 0.24
201132684.01	K2-158b	2	5.90279 ± 0.00233	0.06205 ± 0.00068	0.0123 ± 0.0012	1.27 ± 0.13
201132684.02	K2-158c	2	10.06049 ± 0.00148	0.08853 ± 0.00095	0.0255 ± 0.0016	2.64 ± 0.17
201155177	K2-42	3	6.68796 ± 0.00093	0.06339 ± 0.00070	0.0304 ± 0.0028	2.41 ± 0.23
201160662	–	13	1.5374115 ± 0.0000062	0.02800 ± 0.00054	0.259 ± 0.071	57.13 ± 15.77
201264302	–	4	0.212194 ± 0.000026	0.00532 ± 0.00010	0.0271 ± 0.004	1.25 ± 0.18
201390927	–	2	2.638 ± 0.0003	0.03585 ± 0.00072	0.0265 ± 0.0025	3.04 ± 0.39
201393098	K2-7	3	28.6777 ± 0.0086	0.18752 ± 0.00232	0.0177 ± 0.0018	3.29 ± 0.34
201403446	K2-46	1	19.15454 ± 0.002849	0.14283 ± 0.00182	0.01705 ± 0.00127	2.66 ± 0.21
201407812	–	5	2.8268121	0.04192 ± 0.00060	0.4560	119.51 ± 4.02
201445732	–	13	11.20381 ± 0.00055	0.09748 ± 0.00122	0.0182 ± 0.0027	2.37 ± 0.35
201516974	–	6	36.7099 ± 0.0125	0.23590 ± 0.00833	0.0489 ± 0.0033	31.18 ± 2.50
201546283	K2-27	1	6.771389 ± 0.000062	0.06831 ± 0.00071	0.049112 ± 0.001573	4.70 ± 0.16
201561956	–	13	13.2359 ± 0.0031	0.10587 ± 0.00162	0.0208 ± 0.0046	2.17 ± 0.49
201606542	–	4	0.444372 ± 0.000042	0.01119 ± 0.00011	0.0136 ± 0.002	1.63 ± 0.24
201649426	–	5	27.770388	0.16741 ± 0.00090	0.3722	33.45 ± 0.44
201754305.02	K2-16b	3	7.61856 ± 0.00096	0.06675 ± 0.00071	0.0268 ± 0.0022	1.93 ± 0.16
201754305.01	K2-16c	3	19.077 ± 0.0033	0.12310 ± 0.00131	0.0299 ± 0.003	2.15 ± 0.22
201779067	–	5	27.242912	0.19034 ± 0.00326	0.2367	64.10 ± 1.94
201841433	–	5	12.339133	0.09614 ± 0.00097	0.02881	2.33 ± 0.21
201855371	K2-17	1	17.969079 ± 0.0014	0.11508 ± 0.00085	0.029715 ± 0.003	1.96 ± 0.20
201856786.01	–	13	3.83794 ± 0.00041	0.04178 ± 0.00090	0.0172 ± 0.003	1.46 ± 0.26
201856786.02	–	13	5.24086 ± 0.00094	0.05143 ± 0.00111	0.0166 ± 0.0027	1.41 ± 0.24
201912552	K2-18	3	32.9418 ± 0.0021	0.15444 ± 0.01138	0.0517 ± 0.0021	2.46 ± 0.14
201923289	–	5	0.78214992	0.01616 ± 0.00021	0.01346	1.34 ± 0.25
202634963	–	5	28.707623	0.20176 ± 0.00356	0.2136	44.32 ± 1.25
202675839	–	1	15.466674 ± 0.0016	0.13015 ± 0.00205	$0.12002^{+0.3}_{-0.062}$	21.36 ± 53.40
202821899	–	1	4.474513 ± 0.0003	0.05944 ± 0.00115	0.033719 ± 0.0056	8.32 ± 1.43
203070421	–	5	1.7359447	0.03340 ± 0.00062	0.02551	7.66 ± 0.81
203518244	–	5	0.8411257	0.01893 ± 0.00019	0.01098	2.84 ± 0.65
203533312	–	4	0.17566 ± 0.000183	0.00698 ± 0.00013	0.0248 ± 0.001	7.23 ± 0.35
203616858	–	13	1.68027 ± 0.00011	0.02775 ± 0.00051	0.0207 ± 0.0238	2.85 ± 3.28
203633064	–	13	0.7099504 ± 0.0000013	0.01775 ± 0.00020	0.357 ± 0.079	82.26 ± 18.41
203753577	–	5	3.4007758	0.04702 ± 0.00077	0.06863	9.74 ± 1.53
203771098.02	K2-24b	1	20.885016 ± 0.000438	0.15273 ± 0.00097	0.045111 ± 0.00227	5.71 ± 0.30
203771098.01	K2-24c	1	42.363982 ± 0.000795	0.24473 ± 0.00155	0.061091 ± 0.00174	7.74 ± 0.24
203826436.03	K2-37b	1	4.443774 ± 0.0005	0.05084 ± 0.00056	0.017091 ± 0.01883	1.56 ± 1.72
203826436.01	K2-37c	1	6.429582 ± 0.0003	0.06503 ± 0.00072	0.029105 ± 0.00353	2.66 ± 0.32
203826436.02	K2-37d	1	14.090996 ± 0.001078	0.10973 ± 0.00121	0.027017 ± 0.003572	2.47 ± 0.33
203925865	–	13	8.796890 ± 0.00059	0.08910 ± 0.00084	0.0217 ± 0.003	4.69 ± 0.66
203929178	–	3	1.153886 ± 0.000028	0.02385 ± 0.00044	0.53 ± 0.23	101.86 ± 45.55
204197636	–	13	46.1373 ± 0.00760	0.23732 ± 0.00238	0.033 ± 0.0024	3.06 ± 0.2
204221263.02	K2-38b	3	4.01628 ± 0.00044	0.05009 ± 0.00036	0.01329 ± 0.00099	1.67 ± 0.13

Table 4 – *continued*

EPIC	K2 ID	Reference	P (d)	a (au)	R_p/R_*	R_p ($R_\oplus$)
204221263.01	K2-38c	3	10.56098 ± 0.00081	0.09543 ± 0.00068	0.0195 ± 0.014	2.45 ± 1.76
204914585	–	5	18.357773	0.14669 ± 0.00221	0.01924	2.58 ± 0.34
204991696	–	13	49.8558 ± 0.0035	0.28089 ± 0.00270	0.02222 ± 0.0023	3.11 ± 0.33
205071984.01	K2-32b	1	8.991942 ± 0.000158	0.08206 ± 0.00084	0.056494 ± 0.0013	5.19 ± 0.14
205071984.03	K2-32c	1	20.661623 ± 0.001762	0.14289 ± 0.00148	0.034033 ± 0.001598	3.13 ± 0.15
205071984.02	K2-32d	1	31.715061 ± 0.002567	0.19013 ± 0.0019	0.037299 ± 0.002528	3.43 ± 0.24
205111664	–	5	15.937378	0.11803 ± 0.00112	0.02135	2.24 ± 0.27
205146011	–	13	1.057171 ± 0.000061	0.01985 ± 0.00023	0.0137 ± 0.002	1.41 ± 0.21
205170731	–	13	14.2005 ± 0.0027	0.11034 ± 0.00109	0.0276 ± 0.0053	2.81 ± 0.54
205470347	–	13	1.86732 ± 0.00016	0.02727 ± 0.00016	0.00857 ± 0.00146	0.66 ± 0.11
205503762	–	13	6.4349 ± 0.0012	0.06815 ± 0.00085	0.0152 ± 0.0052	2.24 ± 0.77
205570849	–	3	16.8580 ± 0.0011	0.12831 ± 0.00168	0.047 ± 0.057	6.21 ± 7.53
205618538	–	13	2.167697 ± 0.000022	0.03735 ± 0.00081	0.04472 ± 0.00154	11.38 ± 0.57
205924614	K2-55	3	2.849258 ± 00.000033	0.03536 ± 0.00031	0.0552 ± 0.0013	4.17 ± 0.11
205938820	–	13	4.20773 ± 0.00075	0.04966 ± 0.00052	0.0161 ± 0.0023	1.53 ± 0.22
205944181	–	1	2.475641 ± 0.000057	0.03479 ± 0.00042	$0.055833^{+0.19}_{-0.03}$	5.28 ± 17.97
205950854	K2-168	1	15.853989 ± 0.001415	0.11803 ± 0.00161	0.022489 ± 0.001272	2.21 ± 0.13
205951125	–	13	6.79143 ± 0.0008	0.06487 ± 0.00061	0.0259 ± 0.0064	2.08 ± 0.52
205957328	–	1	14.353438 ± 0.001491	0.11117 ± 0.00077	0.023912 ± 0.004385	2.11 ± 0.39
205998649	–	13	8.3958 ± 0.0028	0.08268 ± 0.00102	0.0181 ± 0.007	3.87 ± 1.50
206024342	–	3	14.637 ± 0.0021	0.11259 ± 0.00194	0.0249 ± 0.0015	2.34 ± 0.15
206026136	K2-57	3	9.0063 ± 0.0013	0.07525 ± 0.00068	0.0308 ± 0.0028	2.24 ± 0.21
206036749	–	3	1.131316 ± 0.00003	0.02226 ± 0.00034	0.047 ± 0.057	3.76 ± 0.23
206038483	K2-60	3	3.002627 ± 0.000018	0.04178 ± 0.00063	0.06191 ± 0.00035	9.87 ± 0.25
206047055	–	13	4.10290 ± 0.00180	0.05208 ± 0.00062	0.0106 ± 0.0022	2.22 ± 0.47
206055981	–	5	20.643928	0.12730 ± 0.00099	0.03129	2.10 ± 0.17
206082454.02	K2-172b	1	14.316941 ± 0.001445	0.11326 ± 0.00110	0.017579 ± 0.001495	1.67 ± 0.14
206082454.01	K2-172c	1	29.62682 ± 0.001607	0.18392 ± 0.00178	0.033824 ± 0.001324	3.21 ± 0.13
206103150.01	WASP-47b	3	4.159221 ± 0.000015	0.05047 ± 0.00058	0.10214 ± 0.0003	12.71 ± 0.27
206103150.02	WASP-47d	3	9.03164 ± 0.00064	0.08464 ± 0.00098	0.026 ± 0.0015	3.24 ± 0.20
206103150.03	WASP-47e	3	0.789518 ± 0.00006	0.01667 ± 0.00019	0.01344 ± 0.00088	1.67 ± 0.12
206114630	–	1	7.445026 ± 0.0003	0.07031 ± 0.00044	0.025337 ± 0.033876	2.29 ± 3.06
206125618	K2-64	3	6.53044 ± 0.00067	0.06671 ± 0.00089	0.0259 ± 0.0017	2.49 ± 0.18
206135682	–	5	5.025831	0.05165 ± 0.00037	0.01961	1.43 ± 0.18
206208956	–	13	5.01038 ± 0.00019	0.05878 ± 0.00120	0.0257 ± 0.0047	4.49 ± 0.85
206245553	K2-73	1	7.495692 ± 0.000283	0.07520 ± 0.00074	0.022901 ± 0.001345	2.65 ± 0.16
206260577	–	13	1.982116 ± 0.000012	0.03254 ± 0.00068	0.157 ± 0.048	31.20 ± 9.59
206369173	–	13	2.018725 ± 0.000066	0.03656 ± 0.00369	0.056 ± 0.018	129.64 ± 46.49
206414361	–	13	3.47722 ± 0.00038	0.03675 ± 0.00023	0.0253 ± 0.0086	1.44 ± 0.49
206417197	–	4	0.442094 ± 0.000086	0.01071 ± 0.00011	0.0138 ± 0.001	1.18 ± 0.09
206476150	–	13	12.19649 ± 0.00082	0.10263 ± 0.00120	0.0192 ± 0.0019	2.10 ± 0.21
210394706.02	–	13	3.16363 ± 0.00029	0.03565 ± 0.00025	0.0222 ± 0.00380	1.41 ± 0.24
210394706.01	–	13	15.0818 ± 0.0025	0.10097 ± 0.00070	0.0326 ± 0.0045	2.08 ± 0.29
210402237	K2-79	1	10.993948 ± 0.000627	0.09707 ± 0.00101	0.027782 ± 0.001543	3.85 ± 0.22
210414957	–	3	0.969967 ± 0.000012	0.02049 ± 0.00020	0.35 ± 0.15	80.64 ± 34.62
210508766.01	K2-83b	3	2.74697 ± 0.00018	0.03182 ± 0.00018	0.0268 ± 0.0019	1.59 ± 0.11
210508766.02	K2-83c	3	9.99767 ± 0.00081	0.07530 ± 0.00043	0.0319 ± 0.0018	1.89 ± 0.11
210559259	–	7	14.2683 ± 0.0012	0.10583 ± 0.00105	$0.02854^{+0.0011}_{-0.00082}$	2.24 ± 0.09
210609658	–	1	14.145239 ± 0.000468	0.12894 ± 0.00310	0.06327 ± 0.00188	22.66 ± 0.91
210629082	–	1	27.353103 ± 0.007472	0.19187 ± 0.00358	0.019308 ± 0.0029	4.13 ± 0.63
210664763	–	13	3.72007 ± 0.00047	0.04714 ± 0.00064	0.01450 ± 0.003	1.56 ± 0.32
210678858.03	–	13	10.0696 ± 0.0013	0.08767 ± 0.00066	0.0190 ± 0.0033	1.66 ± 0.29
210678858.02	–	13	14.8484 ± 0.0011	0.11358 ± 0.00085	0.0302 ± 0.003	2.64 ± 0.26
210678858.01	–	13	31.3537 ± 0.0019	0.18695 ± 0.00140	0.0432 ± 0.003	3.78 ± 0.27
210707130	K2-85	1	0.684553 ± 0.000013	0.01348 ± 0.00011	0.018081 ± 0.001436	1.32 ± 0.11
210718708	K2-86	1	8.775864 ± 0.0009	0.07978 ± 0.00093	0.025082 ± 0.003131	2.27 ± 0.28
210731500	K2-87	3	9.72739 ± 0.00087	0.08914 ± 0.00124	0.0441 ± 0.0032	6.79 ± 0.51
210775710	–	1	59.848566 ± 0.000184	0.29810 ± 0.00401	0.100817 ± 0.001863	11.45 ± 0.27
210857328	K2-177	1	14.155185 ± 0.00315	0.12655 ± 0.00223	0.015987 ± 0.0018	3.07 ± 0.36
210961508	–	4	0.349935 ± 0.000042	0.01050 ± 0.00036	0.0263 ± 0.003	8.47 ± 1.01
211087003.02	–	13	28.29213 ± 0.00126	0.18102 ± 0.00229	0.0338 ± 0.0023	3.84 ± 0.27
211327855	–	13	1.72397 ± 0.00027	0.02727 ± 0.00028	0.0137 ± 0.0038	1.26 ± 0.35
211335816	–	8	4.99	0.06106 ± 0.00103	0.043667 ± 0.0025	8.25 ± 0.53

Table 4 – *continued*

EPIC	K2 ID	Reference	P (d)	a (au)	R_p/R_*	R_p ($R_\oplus$)
211336616	–	8	44.13	0.26941 ± 0.02413	0.020655 ± 0.0025	25.26 ± 3.81
211351816	K2-97	1	8.405276 ± 0.001166	0.09382 ± 0.00307	0.025002 ± 0.003158	12.07 ± 1.66
211355342	K2-181	1	6.894252 ± 0.00043	0.07088 ± 0.00085	0.024829 ± 0.002084	2.87 ± 0.25
211357309	–	9	0.46395 ± 0.00002	0.00921 ± 0.00005	0.017 ± 0.001	0.86 ± 0.05
211359660	K2-182	1	4.736884 ± 0.000075	0.05257 ± 0.00046	0.032108 ± 0.001498	2.77 ± 0.13
211365543	–	8	5.264	0.06275 ± 0.00082	0.009804	1.68 ± 0.43
211390903	–	10	7.757595 ± 0.000822	0.09205 ± 0.00502	0.0251 ± 0.0007	30.42 ± 1.76
211491383	K2-269	1	4.145398 ± 0.001032	0.05213 ± 0.00100	0.008372 ± 0.001162	1.34 ± 0.20
211535327	–	13	20.2244 ± 0.0021	0.13749 ± 0.00166	0.0323 ± 0.0043	3.03 ± 0.41
211562654.03	K2-183b	1	0.469269 ± 0.000026	0.01139 ± 0.00014	$0.027288^{+0.27}_{-0.015}$	2.88 ± 28.54
211562654.01	K2-183c	1	10.793471 ± 0.000803	0.09213 ± 0.00117	0.026365 ± 0.002542	2.79 ± 0.27
211562654.02	K2-183d	1	22.629496 ± 0.001949	0.15093 ± 0.00192	0.026677 ± 0.002712	2.82 ± 0.29
211586387	–	8	35.383	0.22064 ± 0.00402	0.18841 ± 0.00165	2.25 ± 0.19
211611158.02	–	1	52.714072 ± 0.003819	0.27437 ± 0.00257	0.02803 ± 0.00436	2.79 ± 0.44
211611158	K2-185b	1	10.616646 ± 0.0018	0.09427 ± 0.00089	0.013164 ± 0.002118	1.31 ± 0.21
211733267	–	1	8.658168 ± 0.00003	0.07925 ± 0.00083	$0.1921^{+0.114}_{-0.059}$	18.94 ± 11.25
211736305	–	13	14.5616 ± 0.0026	0.11075 ± 0.00138	0.0305 ± 0.0149	2.71 ± 1.33
211736671	K2-108	1	4.73379 ± 0.000153	0.05695 ± 0.00065	0.030069 ± 0.002987	5.75 ± 0.59
211763214	–	1	21.191788 ± 0.003275	0.14294 ± 0.00129	0.015441 ± 0.00162	1.35 ± 0.14
211770696	–	1	16.27284 ± 0.002441	0.12608 ± 0.00175	0.018155 ± 0.00156	2.66 ± 0.24
211800191	–	1	1.106175 ± 0.000009	0.02092 ± 0.00040	0.089351 ± 0.06	11.42 ± 7.67
211816003	K2-272	11	14.453513 ± 0.001783	0.10872 ± 0.00145	0.0336 ± 0.0041	2.98 ± 0.37
211818569	K2-121	1	5.185759 ± 0.000014	0.05269 ± 0.00037	0.10208 ± 0.003964	7.49 ± 0.30
211923431	–	8	29.729	0.18570 ± 0.00199	0.025878 ± 0.0025	3.28 ± 0.33
211945201	–	1	19.491795 ± 0.000516	0.14891 ± 0.00228	0.038014 ± 0.002554	5.81 ± 0.40
211970147	K2-102	12	9.915651 ± 0.001194	0.08342 ± 0.00073	0.0169 ± 0.001	1.35 ± 0.08
211978988	–	1	36.556251 ± 0.004239	0.21767 ± 0.00283	0.026283 ± 0.001964	3.24 ± 0.25
211990866	K2-100	12	1.673915 ± 0.000011	0.02882 ± 0.00028	0.0267 ± 0.0011	3.64 ± 0.16
212006344	K2-122	9	2.21940 ± 0.00007	0.02828 ± 0.00020	0.020 ± 0.001	1.29 ± 0.07
212099230	–	11	7.112273 ± 0.000284	0.07139 ± 0.00131	0.0302 ± 0.0011	3.19 ± 0.12
212110888	K2-34	1	2.995646 ± 0.000006	0.04285 ± 0.00076	0.088002 ± 0.001666	13.93 ± 0.39
212136123	–	8	2.226	0.03192 ± 0.00033	0.026003 ± 0.0025	2.27 ± 0.22
212141021	–	8	2.918	0.03729 ± 0.00041	0.015674 ± 0.0025	1.33 ± 0.21
212159623	–	13	4.70751 ± 0.00065	0.05533 ± 0.00078	0.0139 ± 0.002	1.51 ± 0.22
212164470.01	K2-188b	1	1.742983 ± 0.00026	0.02881 ± 0.00041	0.010407 ± 0.0009	1.36 ± 0.12
212164470.02	K2-188c	1	7.807595 ± 0.000597	0.07827 ± 0.00112	0.021697 ± 0.001430	2.84 ± 0.20
212300977	WASP-55	11	4.465635 ± 0.000023	0.05359 ± 0.00058	0.1223 ± 0.0004	15.09 ± 0.26
212301649	–	8	1.225	0.02145 ± 0.00031	0.014962 ± 0.0025	1.40 ± 0.25
212362217	–	13	0.6962935 ± 0.0000087	0.01514 ± 0.00027	0.0319 ± 0.0369	3.94 ± 4.56
212393193.01	–	8	14.452	0.11948 ± 0.00141	0.0182 ± 0.0025	2.29 ± 0.32
212393193.02	–	8	36.152	0.22018 ± 0.00259	0.0183 ± 0.0025	2.30 ± 0.32
212425103	–	8	0.946	0.01782 ± 0.00024	0.017346 ± 0.0025	1.54 ± 0.23
212432685	–	11	0.531704 ± 0.000035	0.01293 ± 0.00021	0.0169 ± 0.0018	2.18 ± 0.43
212440430	–	8	19.991	0.14224 ± 0.00187	0.023276 ± 0.0025	2.54 ± 0.28
212464382	–	13	4.07337 ± 0.00051	0.04757 ± 0.00046	0.01071 ± 0.00184	0.94 ± 0.16
212495601	–	8	21.677	0.14710 ± 0.00177	0.024596 ± 0.0025	2.71 ± 0.28
212521166	K2-110	1	13.863910 ± 0.000229	0.10373 ± 0.00085	0.033432 ± 0.001766	2.61 ± 0.14
212560683	–	13	13.7043 ± 0.0037	0.11317 ± 0.00114	0.0118 ± 0.0033	1.31 ± 0.37
212585579	–	11	3.021795 ± 0.000094	0.04170 ± 0.00056	0.3876 ± 0.3569	46.56 ± 42.88
212587672	–	1	23.226001 ± 0.003092	0.15929 ± 0.00198	0.021599 ± 0.003624	2.33 ± 0.39
212624936	–	13	11.81387 ± 0.00093	0.09971 ± 0.00128	0.0258 ± 0.0036	2.63 ± 0.37
212639319	–	1	13.843725 ± 0.000948	0.12740 ± 0.00167	$0.037754^{+0.297}_{-0.0096}$	11.05 ± 86.92
212645891	–	1	0.328152 ± 0.000001	0.00934 ± 0.00018	$0.136972^{+0.113}_{-0.06}$	17.05 ± 14.07
212646483	–	8	8.253	0.08348 ± 0.00122	0.029071 ± 0.0025	6.98 ± 0.66
212652418	–	13	19.1324 ± 0.0031	0.14091 ± 0.00202	0.0186 ± 0.0022	2.78 ± 0.34
212672300	K2-194	1	39.721386 ± 0.0057	0.24073 ± 0.00258	0.026065 ± 0.002509	3.90 ± 0.39
212686205	K2-128	1	5.675814 ± 0.000427	0.05520 ± 0.00050	0.016952 ± 0.00133	1.22 ± 0.10
212688920	–	8	62.841	0.30670 ± 0.00604	0.231222 ± 0.0025	27.02 ± 0.62
212689874.01	K2-195b	1	15.853543 ± 0.00079	0.12127 ± 0.00172	0.029741 ± 0.001265	3.20 ± 0.15
212689874.02	K2-195c	1	28.482786 ± 0.00731	0.17922 ± 0.00257	0.026054 ± 0.0024	2.81 ± 0.26
212779596.01	K2-199b	1	3.225423 ± 0.000071	0.03811 ± 0.00035	0.025852 ± 0.002447	1.89 ± 0.18
212779596.02	K2-199c	1	7.374497 ± 0.000118	0.06614 ± 0.00060	0.038968 ± 0.002060	2.86 ± 0.15

Table 4 – *continued*

EPIC	K2 ID	Reference	P (d)	a (au)	R_p/R_*	R_p ($R_\oplus$)
212803289	K2-99	1	18.248708 ± 0.000634	0.15352 ± 0.00168	0.042431 ± 0.001169	12.42 ± 0.48
212828909	K2-200	1	2.849883 ± 0.000188	0.03724 ± 0.00027	0.015799 ± 0.001590	1.33 ± 0.13
213408445	–	13	2.49686 ± 0.00022	0.04315 ± 0.00386	0.072 ± 0.022	301.12 ± 94.83
213546283	–	1	9.770186 ± 0.000325	0.08877 ± 0.00103	0.029436 ± 0.0015	3.73 ± 0.20
213703832	–	11	0.515513 ± 0.000024	0.01397 ± 0.00157	0.0409 ± 0.0096	50.02 ± 13.08
213840781	–	11	12.364531 ± 0.000375	0.10365 ± 0.00208	0.4363 ± 0.2602	60.98 ± 36.40
214419545	–	13	9.40172 ± 0.00048	0.08572 ± 0.00096	0.016 ± 0.0021	2.36 ± 0.31
214630761	–	13	1.236438 ± 0.000022	0.02620 ± 0.00050	0.143 ± 0.04	48.41 ± 13.94
214741009	–	11	7.269622 ± 0.000521	0.09463 ± 0.00400	0.4156 ± 0.3808	419.79 ± 386.31
214888033	–	13	7.457597 ± 0.000096	0.07353 ± 0.00086	0.077 ± 0.015	9.42 ± 1.84
214984368	–	13	0.2633809 ± 0.000003	0.01066 ± 0.00119	0.090 ± 0.021	440.29 ± 137.57
215125108	–	13	0.738067 ± 0.000026	0.01837 ± 0.00149	0.095 ± 0.027	232.37 ± 73.82
215175768	–	13	1.726115 ± 0.000098	0.02788 ± 0.00040	0.0610 ± 0.021	6.28 ± 2.17
215364084	–	13	2.74324 ± 0.00017	0.04290 ± 0.00192	0.0526 ± 0.0265	30.33 ± 15.39
215381481	–	13	0.533393 ± 0.000027	0.01352 ± 0.00096	0.01206 ± 0.00232	72.96 ± 15.99
216111905	–	13	3.02030 ± 0.00032	0.04040 ± 0.00045	0.0410 ± 0.020	5.73 ± 2.80
216363472	–	13	8.69290 ± 0.00085	0.08138 ± 0.00108	0.0154 ± 0.0170	1.68 ± 1.86
216405287	K2-202	1	3.405164 ± 0.000126	0.04334 ± 0.00061	0.023171 ± 0.001335	2.28 ± 0.14
216494238	K2-280	1	19.894641 ± 0.002898	0.14649 ± 0.00183	0.047857 ± 0.002267	6.74 ± 0.35
218195416	–	13	0.4951253 ± 0.0000031	0.01447 ± 0.00023	0.1410 ± 0.0130	33.41 ± 3.54
218300572	–	13	1.589843 ± 0.000013	0.03266 ± 0.00094	0.114 ± 0.033	43.20 ± 12.86
219388192	–	1	5.292605 ± 0.000031	0.05860 ± 0.00076	0.094335 ± 0.000852	10.92 ± 0.22
219480273	–	13	26.48370 ± 0.0051	0.17671 ± 0.00195	0.0132 ± 0.0033	2.03 ± 0.51
219800881	K2-231	13	13.84457 ± 0.00154	0.11357 ± 0.00156	0.0248 ± 0.0018	2.74 ± 0.20
220170303	K2-203	1	9.695101 ± 0.001334	0.08375 ± 0.00062	0.01647 ± 0.003246	1.37 ± 0.27
220186645	K2-204	1	7.055784 ± 0.000650	0.07246 ± 0.00090	0.023711 ± 0.00094	3.50 ± 0.18
220198551	–	13	0.7988453 ± 0.0000083	0.01593 ± 0.00011	0.079 ± 0.035	7.26 ± 3.22
220209578	–	11	8.904519 ± 0.000205	0.08322 ± 0.00115	0.3805 ± 0.3287	44.04 ± 38.07
220245303	–	1	3.680340 ± 0.000359	0.04394 ± 0.00032	0.012565 ± 0.0022	1.05 ± 0.18
220282718	–	13	0.5551606 ± 0.0000058	0.01364 ± 0.00019	0.0630 ± 0.034	11.21 ± 6.06
220322327	–	13	3.313470 ± 0.00024	0.04074 ± 0.00047	0.042 ± 0.033	3.62 ± 2.85
220341183	K2-213	1	8.130870 ± 0.001799	0.08241 ± 0.00088	0.011526 ± 0.001564	1.66 ± 0.23
220400100	–	7	10.7946 ± 0.0019	0.08817 ± 0.00080	$0.0314^{+0.0039}_{-0.0019}$	2.49 ± 0.31
220431824	–	13	9.073266 ± 0.000037	0.08652 ± 0.00102	0.1213 ± 0.0026	23.71 ± 0.71
220436189	–	13	13.60940 ± 0.00330	0.09313 ± 0.00064	0.0396 ± 0.0045	2.42 ± 0.28
220436208	–	11	5.235714 ± 0.000316	0.05920 ± 0.00071	0.0337 ± 0.0034	4.38 ± 0.46
220459477	–	13	2.38098 ± 0.00018	0.03250 ± 0.00039	0.0215 ± 0.0038	1.82 ± 0.32
220470563	–	13	7.30383 ± 0.00043	0.06855 ± 0.00049	0.02790 ± 0.0036	2.23 ± 0.29
220481411	K2-216	1	2.174789 ± 0.000039	0.02953 ± 0.00029	0.023117 ± 0.001166	1.74 ± 0.09
220621788	K2-220	1	13.682511 ± 0.000721	0.10864 ± 0.00103	0.021843 ± 0.001610	2.43 ± 0.18
220629489	K2-283	11	1.921076 ± 0.000050	0.02890 ± 0.00028	0.0404 ± 0.0048	3.59 ± 0.43
220639177	–	13	7.14238 ± 0.00069	0.06660 ± 0.00067	0.0236 ± 0.0057	1.86 ± 0.45
220643470	–	1	2.653230 ± 0.000089	0.04349 ± 0.00461	0.041582 ± 0.002685	134.86 ± 21.21
220674823.01	–	1	0.571299 ± 0.000015	0.01329 ± 0.00017	0.016876 ± 0.00137	1.82 ± 0.15
220674823.02	–	1	13.339746 ± 0.001089	0.10854 ± 0.00138	0.027358 ± 0.003262	2.95 ± 0.35
228725791.01	K2-247b	2	2.25021 ± 0.00036	0.02989 ± 0.00027	0.0283 ± 0.0025	2.10 ± 0.19
228725791.02	K2-247c	2	6.49424 ± 0.00260	0.06059 ± 0.00056	0.0292 ± 0.0032	2.17 ± 0.24
228734889	–	1	48.249552 ± 0.000173	0.25637 ± 0.00368	0.172572 ± 0.00245	19.60 ± 0.53
228735255	K2-140	1	6.569213 ± 0.000020	0.06909 ± 0.00089	0.114173 ± 0.000560	12.72 ± 0.32
228736155	K2-226	1	3.271106 ± 0.000369	0.04227 ± 0.00071	0.016535 ± 0.001862	1.66 ± 0.19
228754001	K2-132	1	9.173866 ± 0.001534	0.09237 ± 0.00294	0.029103 ± 0.001475	12.43 ± 0.73
229017395	K2-258	2	19.09210 ± 0.00633	0.13931 ± 0.00174	0.0210 ± 0.0014	3.12 ± 0.22
247047370	–	7	4.20566 ± 0.00018	0.04910 ± 0.00064	0.0267 ± 0.0029	2.50 ± 0.27
247063356	–	7	9.7051 ± 0.0016	0.09163 ± 0.00119	0.0197 ± 0.0020	2.37 ± 0.24

and is about 3σ smaller than the radius given by Grunblatt et al. (2018).

Fig. 7 shows the comparison between planet-candidate radii derived in this work and the values from the literature sources (as per the references given in Table 4). The right-hand panel details planets smaller than $4\,R_\oplus$ and differentiates those having previously published radius estimates derived from spectroscopy versus photometry. We also show results from Kruse et al. (2019), who used stellar radii determined from *Gaia* DR2. No systematic trend is evident in our revised planet radii. Of the 125 candidates with published spectroscopically derived radii, for which we obtain $R_p < 22\,R_\oplus$, our results are 4σ different for five of them. Four

Table 5. Candidates larger than 22 $R_\oplus$. These candidates are highly likely to be false positives.

EPIC	R_p ($R_\oplus$)	Comments
201160662	57.13 ± 15.77	*Gaia* RV error 4.5σ too large
201407812	119.51 ± 4.02	Double-lined binary. *Gaia* RV error 3.0σ too large
201516974	31.18 ± 2.50	*Gaia* RV error 4.0σ too large. Seismic log $g = 2.934 \pm 0.010$
201649426	33.45 ± 0.44	*Gaia* RV error 4.6σ too large
201779067	64.10 ± 1.94	*Gaia* RV error 8.2σ too large
202634963	44.32 ± 1.25	Double-lined binary
203633064	82.26 ± 18.41	–
203929178	101.86 ± 74.42	*Gaia* astrometric noise 419σ
206260577	31.20 ± 9.59	–
206369173	129.64 ± 46.49	log $g = 1.69 \pm 0.15$
210414957	80.64 ± 34.62	Large uncertainty from R_p/R_*
210609658	22.66 ± 0.91	*Gaia* RV error 3.1σ too large
211336616	25.26 ± 3.81	log $g = 2.06 \pm 0.18$
211390903	30.42 ± 1.76	log $g = 2.89 \pm 0.19$. Seismic log $g = 2.626 \pm 0.022$
212585579	46.56 ± 42.88	*Gaia* RV error 3.1σ too large
212688920	27.02 ± 0.62	–
213408445	301.12 ± 94.83	log $g = 1.21 \pm 0.19$
213703832	50.02 ± 13.08	log $g = 2.34 \pm 0.21$.
213840781	60.98 ± 36.40	Large uncertainty from R_p/R_*.
214630761	48.41 ± 13.94	–
214741009	419.79 ± 386.31	log $g = 2.25 \pm 0.21$.
214984368	440.29 ± 137.57	log $g = 1.50 \pm 0.18$
215125108	232.37 ± 73.82	log $g = 2.01 \pm 0.21$
215364084	30.33 ± 15.39	log $g = 3.08 \pm 0.22$
215381481	72.96 ± 15.99	log $g = 0.73 \pm 0.19$
218195416	33.41 ± 3.54	–
218300572	43.20 ± 12.86	–
220209578	122.05 ± 105.52	Large uncertainty from R_p/R_*.
220431824	23.71 ± 0.71	–
220643470	134.86 ± 21.21	log $g = 1.51 \pm 0.13$

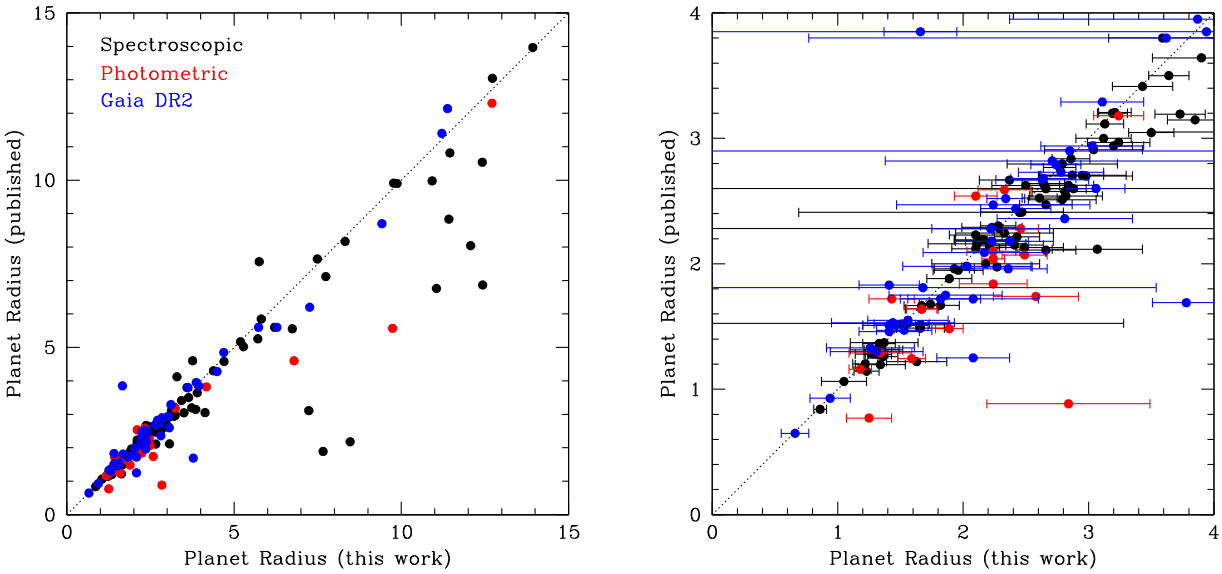

Figure 7. Left-hand panel: Comparison of our derived planetary radii with those from the literature. Error bars have been omitted for clarity. Right-hand panel: Same, but for planet candidates smaller than $4R_\oplus$. The red points denote published radii derived from photometry, whilst black points are those published values derived from spectroscopy and blue points are from *Gaia* DR2. Large error bars arise from uncertainties in the radius ratio R_p/R_* rather than the stellar radii.

of those (EPIC 203070421, 203533312, 210961508, 228754001) orbit evolved stars with log g ranging from 3.31 to 3.78 and radii from 2.67 to 3.91 $R_\odot$. This results in larger inferred planetary radii, turning some potentially rocky worlds into gas giants. Our revised radii for these planet candidates lie in the realm of Saturn and Jupiter, and so remain eminently plausible.

A large-scale analysis of spectroscopic parameters for stars hosting *Kepler* planet candidates revealed a 'radius gap' (Fulton

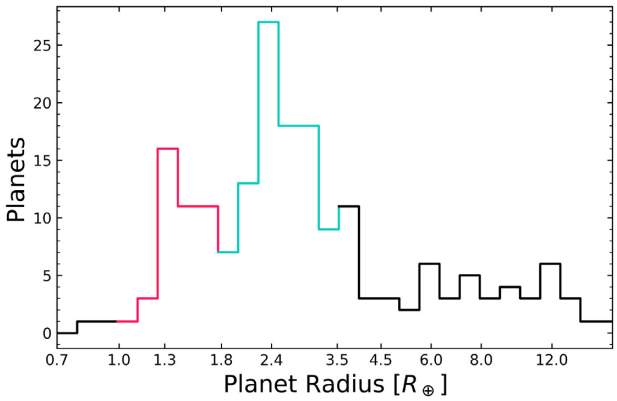

Figure 8. Histogram of our revised planet radii. Red: Rocky planets. Cyan: Gaseous 'mini-Neptune' planets. The radius gap noted by Fulton et al. (2017) and Hardegree-Ullman et al. (2020) is evident.

et al. 2017), with planets of 1.5–2.0$R_\oplus$ apparently depleted by more than a factor of two. Subsequent studies have confirmed that result; Van Eylen et al. (2018) used 117 planets with median radius uncertainties of 3.3 per cent as derived from asteroseismology to further characterize the radius gap. In Fig. 8, we show the distribution of planet-candidate radii from our K2-HERMES sample. Our sample, although smaller than the surveys conducted by Fulton et al. (2017) and Hardegree-Ullman et al. (2020), also sees a drop off in exoplanetary candidates and confirmed exoplanets centred around 1.8$R_\oplus$. Hardegree-Ullman et al. (2020) in particular showed that K2 planet candidates were depleted within a radius gap centred at 1.9 $R_\oplus$.

In Fig. 9, we explore the radius gap in more detail, showing the planet radii as a function of both orbital period and semimajor axis. The radius gap was shown by Van Eylen et al. (2018) to have a slope dependent on orbital period, with a slope of $\frac{\mathrm{dlog}R}{\mathrm{dlog}P}$ of approximately −1/9, a value corroborated by Gupta & Schlichting (2019) and illustrated in Fig. 9. In this Figure, we show as filled circles those

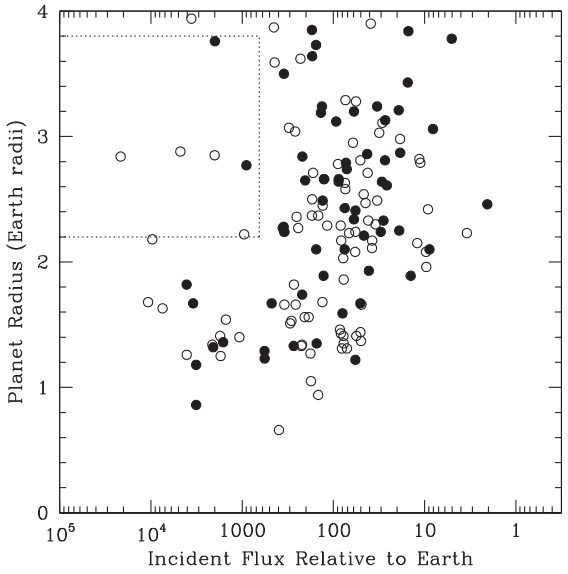

Figure 10. Planet radius versus incident flux, in Earth units. The filled circles indicate planets for which we obtain radius estimates at better than 10 per cent precision. The dashed lines enclose the hot Super-Earth desert (Lundkvist et al. 2016).

95 planets for which we derive radii with precision of 10 per cent or better. The K2 sample investigated here gave consistent results for the shape and slope of this evaporation valley, with the exception of four candidates. These planets (EPIC 206082454, 201754305.02, 210508766.02, 228725791.01) appear as filled circles falling on the dashed line in the right-hand panel of Fig. 9. These candidates have radii with precisions of better than 10 per cent. Interestingly, three of these four are members of multiple systems. Fig. 10 gives the planet radius as a function of incident stellar flux (Table 3). The hot super-Earth desert postulated by Lundkvist et al. (2016) is shown as a box enclosing the region between 2.2–3.8 $R_\oplus$ and S_{inc} >650 $F_\oplus$. Near

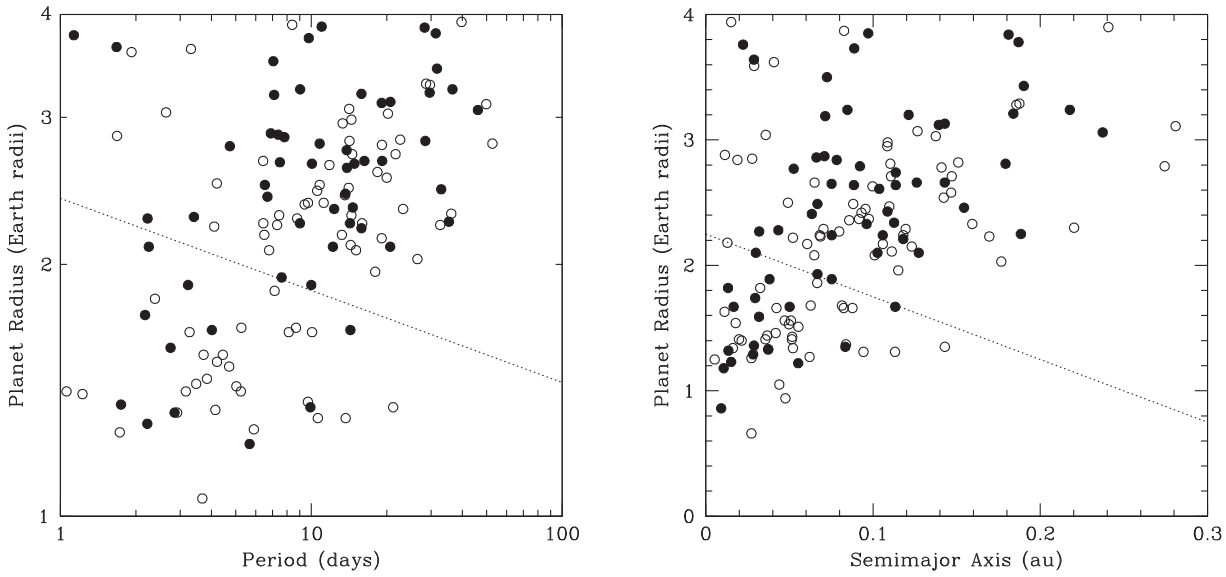

Figure 9. Left-hand panel: Planet radius versus orbital period; the filled circles indicate planets for which we obtain radius estimates at better than 10 per cent precision. The dashed line indicates the slope in the radius valley as noted by Van Eylen et al. (2018) and Gupta & Schlichting (2019). Right-hand panel: Planet radius versus semimajor axis, as computed from the *K*2 period and our derived host-star masses. The symbols have the same meaning as in the left-hand panel.

the edges of this region lie only two planet candidates with radius estimates better than 10 per cent precision, EPIC 206036749.01 and EPIC 211359660.01.

4 SUMMARY AND CONCLUSION

In this work, we have presented a self-consistent catalogue of spectroscopic host-star parameters for 199 *K*2 planet hosts, and the derived physical parameters of 224 planets. We use the revised radii for these planet candidates to cast doubt on 30 as-yet-unconfirmed planets, and we strongly suspect those to be false positives. We also examine the distribution of planet radii as a function of period, showing that the radius gap of the main *Kepler* sample is indeed also evident in this *K*2 sample. The slope of the radius valley is also consistent with that obtained for the *Kepler* planets by Van Eylen et al. (2018) and Gupta & Schlichting (2019), with a handful of interesting exceptions.

In addition to the 30 planet candidates which are rendered implausible based on their revised host-star parameters, our results confirm the small radii of a handful of nearly Earth-sized planets. They are EPIC 205470347 ($0.66 \pm 0.11\,R_\oplus$), EPIC 211357309 ($0.86 \pm 0.05\,R_\oplus$), EPIC 212464382 ($0.94 \pm 0.16\,R_\oplus$), and EPIC 220245303 ($1.05 \pm 0.18\,R_\oplus$). However, as shown in Table 3, these Earth-sized planets are far from Earth-like, receiving stellar flux hundreds of times greater than the Earth.

Our results highlight the importance of accurate stellar parametrization in the characterization of newly discovered exoplanets. Fortunately, with surveys like GALAH and instruments like HERMES it is possible to rapidly characterize large numbers of potential exoplanet host stars. In the coming decade, as the exoplanet discovery rate continues to climb, such surveys will prove pivotal in ensuring the fidelity of the exoplanet catalogue.

ACKNOWLEDGEMENTS

DS is supported by Australian Research Council Future Fellowship FT1400147. SS is funded by University of Sydney Senior Fellowship made possible by the office of the Deputy Vice Chancellor of Research, and partial funding from Bland-Hawthorn's Laureate Fellowship from the Australian Research Council. SLM acknowledges support from the Australian Research Council through Discovery Project grant DP180101791. SB acknowledges funds from the Alexander von Humboldt Foundation in the framework of the Sofja Kovalevskaja Award endowed by the Federal Ministry of Education and Research. This research has been supported by the Australian Research Council (grants DP150100250 and DP160103747). Parts of this research were supported by the Australian Research Council (ARC) Centre of Excellence for All Sky Astrophysics in 3 Dimensions (ASTRO 3D), through project number CE170100013. LC is supported by Australian Research Council Future Fellowship FT160100402. This research has made use of NASA's Astrophysics Data System (ADS), and the SIMBAD data base, operated at CDS, Strasbourg, France. This research has made use of the NASA Exoplanet Archive, which is operated by the California Institute of Technology, under contract with the National Aeronautics and Space Administration under the Exoplanet Exploration Program. We thank the Australian Time Allocation Committee for their generous allocation of AAT time, which made this work possible. We acknowledge the traditional owners of the land on which the AAT stands, the Gamilaraay people, and pay our respects to elders past, present, and emerging.

REFERENCES

Adams E. R., Jackson B., Endl M., 2016, AJ, 152, 47
Albrecht S. et al., 2012, ApJ, 757, 18
Batalha N. M. et al., 2013, ApJS, 204, 24
Borucki W. J. et al., 2010, Science, 327, 977
Bouchy F. et al., 2005, A&A, 444, L15
Buder S. et al., 2018, MNRAS, 478, 4513
Burgasser A. J. et al., 2010, ApJ, 725, 1405
Campbell B., Walker G. A. H., Yang S., 1988, ApJ, 331, 902
Chandler C. O., McDonald I., Kane S. R., 2016, AJ, 151, 59
Charbonneau D. et al., 2009, Nature, 462, 891
Čotar K. et al., 2019, MNRAS, 483, 3196
Čotar K. et al., 2019, MNRAS, 487, 2474
Crossfield I. J. M. et al., 2016, ApJS, 226, 7
De Silva G. M. et al., 2015, MNRAS, 449, 2604
Dotter A., 2016, ApJS, 222, 8
Dressing C. D. et al., 2017, AJ, 154, 207
Duong L. et al., 2018, MNRAS, 476, 5216
Freeman K. C., 2012, in Aoki W., ed., ASP Conf. Ser. Vol. 458, Galactic Archaeology: Near-field Cosmology and the Formation of the Milky Way. Astron. Soc. Pac., San Francisco, p. 393
Fressin F. et al., 2013, ApJ, 766, 81
Fulton B. J. et al., 2017, AJ, 154, 109
Gaia Collaboration 2018, A&A, 616, A1
Gao X. et al., 2018, MNRAS, 481, 2666
Grunblatt S. K. et al., 2018, ApJ, 861, L5
Gupta A., Schlichting H. E., 2019, MNRAS, 487, 24
Harakawa H. et al., 2015, ApJ, 806, 5
Hardegree-Ullman K. K. et al., 2019, AJ, 158, 75
Hardegree-Ullman K. K. et al., 2020, ApJS, 247, 28
Hellier C., Anderson D. R., Collier-Cameron A., Miller G. R. M., Queloz D., Smalley B., Southworth J., Triaud A. H. M. J., 2011, ApJ, 730, L31
Hon M., Stello D., Yu J., 2018, MNRAS, 476, 3233
Howard A. W. et al., 2012, ApJS, 201, 15
Howell S. B. et al., 2014, PASP, 126, 398
Huber D., Stello D., Bedding T. R., Chaplin W. J., Arentoft T., Quirion P.-O., Kjeldsen H., 2009, Commun. Asteroseismol., 160, 74
Huber D. et al., 2011, ApJ, 743, 143
Huber D. et al., 2016, ApJS, 224, 2
Johns D. et al., 2018, ApJS, 239, 14
Kalas P. et al., 2008, Science, 322, 1345
Kane S. R., 2014, ApJ, 782, 111
Kane S. R., 2018, ApJ, 861, L21
Kane S. R., Gelino D. M., 2011, ApJ, 741, 52
Kane S. R., Kopparapu R. K., Domagal-Goldman S. D., 2014, ApJ, 794, L5
Kane S. R. et al., 2016, ApJ, 830, 1
Kane S. R. et al., 2019, J. Geophys. Res., 124, 2015
Katz D. et al., 2019, A&A, 622, A205
Kempton E. M.-R. et al., 2018, PASP, 130, 114401
Kopparapu R. K. et al., 2013, ApJ, 765, 131
Kopparapu R. K., Ramirez R. M., SchottelKotte J., Kasting J. F., Domagal-Goldman S., Eymet V., 2014, ApJ, 787, L29
Kos J. et al., 2017, MNRAS, 464, 1259
Kos J. et al., 2018, MNRAS, 473, 4612
Kos J. et al., 2018, MNRAS, 480, 5242
Kruse E., Agol E., Luger R., Foreman-Mackey D., 2019, ApJS, 244, 11
Lagrange A.-M. et al., 2009, A&A, 493, L21
Latham D. W., Mazeh T., Stefanik R. P., Mayor M., Burki G., 1989, Nature, 339, 38
Livingston J. H. et al., 2018b, AJ, 156, 78
Luger R., Agol E., Kruse E., Barnes R., Becker A., Foreman-Mackey D., Deming D., 2016, AJ, 152, 100
Lundkvist M. S. et al., 2016, Nat. Commun., 7, 11201
Mann A. W. et al., 2017, AJ, 153, 64
Marois C., Macintosh B., Barman T., Zuckerman B., Song I., Patience J., Lafrenière D., Doyon R., 2008, Science, 322, 1348

Marois C., Zuckerman B., Konopacky Q. M., Macintosh B., Barman T., 2010, Nature, 468, 1080
Martell S. L. et al., 2017, MNRAS, 465, 3203
Masset F. S., Papaloizou J. C. B., 2003, ApJ, 588, 494
Masuda K., 2014, ApJ, 783, 53
Mayo A. W. et al., 2018, AJ, 155, 136
Mayor M., Queloz D., 1995, Nature, 378, 355
Morton T. D., 2015, Isochrones: Stellar model grid package, record ascl:1503.010
Mullally F. et al., 2015, ApJS, 217, 31
Nardiello D., Libralato M., Bedin L. R., Piotto G., Borsato L., Granata V., Malavolta L., Nascimbeni V., 2016, MNRAS, 463, 1831
Ostberg C., Kane S. R., 2019, AJ, 158, 195
Petigura E. A. et al., 2017, AJ, 153, 142
Pope B. J. S., Parviainen H., Aigrain S., 2016, MNRAS, 461, 3399
Quillen A. C. et al., 2018, MNRAS, 478, 228
Raetz S., Heras A. M., Fernández M., Casanova V., Marka C., 2019, MNRAS, 483, 824
Salaris M., Chieffi A., Straniero O., 1993, ApJ, 414, 580
Schmitt J. R. et al., 2016, AJ, 151, 159
Sharma S., Stello D., Bland-Hawthorn J., Huber D., Bedding T. R., 2016, ApJ, 822, 15
Sharma S. et al., 2018, MNRAS, 473, 2004
Sharma S. et al., 2019, MNRAS, 490, 5335
Simpson J. D. et al., 2016, MNRAS, 459, 1069
Sinukoff E. et al., 2016, ApJ, 827, 78
Skrutskie M. F. et al., 2006, AJ, 131, 1163
Sliski D. H., Kipping D. M., 2014, ApJ, 788, 148
Stello D. et al., 2017, ApJ, 835, 83
Tamuz O. et al., 2008, A&A, 480, L33
Van Eylen V., Agentoft C., Lundkvist M. S., Kjeldsen H., Owen J. E., Fulton B. J., Petigura E., Snellen I., 2018, MNRAS, 479, 4786
Vanderburg A. et al., 2016, ApJS, 222, 14
Vogt S. S. et al., 2010, ApJ, 708, 1366
Winn J. N., Fabrycky D. C., 2015, ARA&A, 53, 409
Winn J. N. et al., 2011, ApJ, 737, L18
Wittenmyer R. A., Endl M., Cochran W. D., Levison H. F., 2007, AJ, 134, 1276
Wittenmyer R. A. et al., 2017, AJ, 154, 274
Wittenmyer R. A. et al., 2018, AJ, 155, 84
Wolszczan A., Frail D. A., 1992, Nature, 355, 145
Wright J. T., Marcy G. W., Howard A. W., Johnson J. A., Morton T. D., Fischer D. A., 2012, ApJ, 753, 160
Yu J., Huber D., Bedding T. R., Stello D., Hon M., Murphy S. J., Khanna S., 2018, ApJS, 236, 42
Zink J. K. et al., 2019, Res. Notes Am. Astron. Soc., 3, 43
Zwitter T. et al., 2018, MNRAS, 481, 645
Žerjal M. et al., 2019, MNRAS, 484, 4591

SUPPORTING INFORMATION

Supplementary data are available at *MNRAS* online.

Table 2. Spectroscopic and derived stellar parameters.
Table 3. Planetary insolation and habitable zone boundaries.

Please note: Oxford University Press is not responsible for the content or functionality of any supporting materials supplied by the authors. Any queries (other than missing material) should be directed to the corresponding author for the article.

This paper has been typeset from a TEX/LATEX file prepared by the author.